

**TITLE: PPAR $\gamma$  Deficiency Exacerbates Fibrotic Response to Mycobacteria Peptide in Murine Sarcoidosis Model**

**AUTHORS: Amrita Malur, Barbara Muller-Borer, Gina Murray, Kim Kew, Chuanzhen Zhou, Josh Russell, Jacob L Jones, Christopher J Wingard, Barbara P Barna, and Mary Jane Thomassen**

ONLINE DATA SUPPLEMENT

Supplemental Methods:

**Characterization of MWCNT.** Scanning electron microscope (SEM) images were obtained using a JEOL model JSM-7600 at 5 kV electron energy and working distance of 6.2 mm. The diameters of the MWCNTs in vacuum were characterized by measuring the diameters of all singularly identifiable MWCNTs from the SEM images. The MWCNTs were dispersed in solutions containing PBS/surfactant at 2mg/ml concentration; 40  $\mu$ L ESAT-6 was added to 460  $\mu$ L of MWCNT/PBS surfactant. The size distribution of the MWCNTs in solution and zeta potential was characterized using a Malvern Zetasizer Nano ZS. The solutions were ultrasonicated for 45 minutes and equilibrated to 25°C for two minutes prior to testing. Raman spectroscopy was performed using a Horiba XploRA PLUS Confocal Raman Microscope using a 532 nm laser with 600 l/mm grating.

**Characterization of Bronchoalveolar Lavage (BAL) Cells.** Leukocyte differential counts of BAL cells were calculated from cytopspins (100 cells/40x high power field x 3 fields) as previously described (10). Aliquots of BAL cells were centrifuged and frozen for qPCR evaluation as previously described (20). Total RNA was extracted from BAL cells by miRNeasy protocol (Qiagen, Valencia, CA). Expression of mRNA was determined by real time qPCR using the ABI Step One Plus Real Time PCR system (Applied Biosystems, Foster City, CA.). Primer-probe sets for CCL2 (PPM03151G), Osteopontin (OPN) (PPM03648C), Fibronectin 1 (Fn1) (PPM037886A), IL-13 (PPM03021B), TGF $\beta$  (PPM02991B), MMP9 (PPM03661C), PDGF $\alpha$  (PPM03103E), CD3 (PPM04598A), SMAD3 (PPM04461C) and GAPDH (PPM02946E) as the housekeeping gene were obtained from Qiagen, Germantown, MD. Data were expressed as fold change in mRNA expression compared to control values as previously described (10;10).

**Histological Analysis.** Hematoxylin and Eosin stained sections of 7 $\mu$ m lung from each of the experimental mice were assigned a score of between 0 and 6 by two independent investigators using the following scoring system: (score 0) – no granulomas or aggregates of macrophages seen; (score 1) - few small groups of macrophages but no well-formed granulomas; (score 2) - scattered small granulomas not easily seen on scanning power (20X); (score 3) - scattered small granulomas easily seen on scanning power (20X); (score 4) - scattered small granulomas with occasional larger granulomas seen on scanning power (20X); (score 5) - numerous large granulomas easily seen on scanning power, numerous large granulomas which cover most areas of the lung (20X); (score 6). Scores obtained were averaged for the final analysis.

**Laser Capture Microdissection (LCM).** Mice were sacrificed, and lungs were inflated with diluted Tissue-Tek OCT (Sakura Finetek), 50% (v/v) in RNase-free PBS in 1:3 ratio, and immediately frozen on dry ice. Tissue sections (7  $\mu$ m) were processed and stained. A Zeiss PALM IV LCM was utilized to dissect individual granulomas from frozen lung tissue sections previously inspected for granuloma pathology. LCM was performed to extract granulomas, non-granuloma lung (unaffected lung tissue) and normal lung tissue. Excised tissues were collected into Qiazol buffer (Qiagen). RNA was extracted, converted into cDNA, then analyzed by quantitative PCR for gene expression (10).

**NanoLiquid Chromatography/Mass Spectrometry Method.** An Eksigent 425 nanoLC/AB Sciex 5600+ Triple Time-of-flight mass spectrometer (nano-LC/MS) was used to measure ESAT-6 in lung tissue samples. Mobile phase consisted of A:water with 0.1% formic acid and B:acetonitrile with 0.1% formic acid. The samples were injected using a trap and elute method. First 5  $\mu$ L of sample was injected on a ChromXP C18 trapping column at a flow rate of 3  $\mu$ L/min using water with 0.1% formic acid for 10 min than the valve switched to elute the sample on a ChromXP C18CL column, 150 x 0.3 mm 3  $\mu$ m maintained at 25°C. The nano-LC gradient profile

started at 3% B, increased to 33% B over 30 min, increased to 80% B for 1 min and held for 3 min, decreased back to 3% B for 1 min and held at 3% B for 10 min for a total run time of 45 min. The flow rate was 300 nL/min and introduced into the mass spectrometer using a New Objective Digital PicoView 450 electrospray nano source. The spray position was optimized prior to sample introduction and monitored via camera.

The mass spectrometry (MS) method was set up to collect data in positive ionization mode and two experiments were used for data collection. For experiment 1, the time-of-flight (TOF MS) scan range was from 400 to 1500 with an accumulation time of 0.250 sec for a total time of 40 min. The MS source parameters were set with a declustering potential to 100 V, collision energy 10, source gas 10, curtain gas 25, ion spray voltage 2.5 kV, and an interface heater temperature 150°C. For the second experiment, an independent data acquisition (IDA) was utilized to collect MSMS information. The IDA criteria were set for ions greater than 400 and less than 1250 with a charge state range from 2-4 that exceed signal of 150 counts/sec. Twenty candidates were selected to monitor per cycle and excluding former target ions every 4 seconds. The IDA experiment was utilized to analyze the fragmentation pattern of the ESAT-6. Mass calibration was conducted using a PepCal mix and was conducted every 5 samples.

**Data Analysis for Mass Spectrometry.** Data analysis was conducted using PeakView 2.2 (AB Sciex, Redwood City, CA). ESAT-6 fragments were identified in BioTools application in PeakView 2.2.

**Figure E1.**

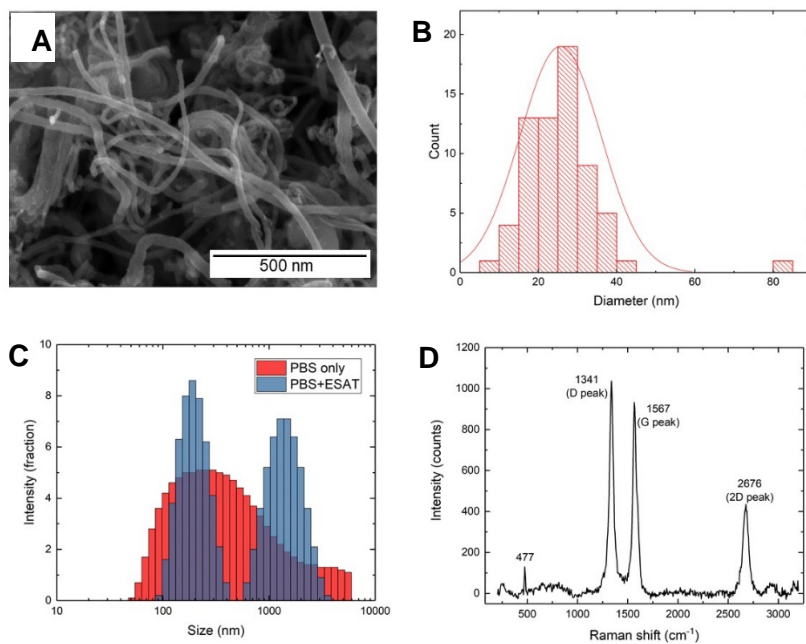


**Figure E1. Characterization of Carbon Nanotubes.** (A) SEM image of the CNTs at 100,000 times magnification. (B) Histogram and fit to Gaussian distribution of the measured cross-sectional diameters of the singularly identifiable CNTs from the SEM images. (C) Size distributions from DLS for the two solutions. (D) Raman spectra of CNTs in ambient conditions, identifying the characteristic CNT peaks.